J Appl Electrochem (2012) 42:595–606
DOI 10.1007/s10800-012-0436-y

ORIGINAL PAPER

Influence of triethylamine on the anodic dissolution characteristics of Ni, Cu and their alloys in non-aqueous solvents containing fluoride media: voltammetric and surface morphologic study

S. Sathyamoorthi · KR. Saravanan · D. Velayutham · V. Suryanarayanan

Received: 11 April 2012 / Accepted: 21 May 2012 / Published online: 8 June 2012

Abstract Multisweep cyclic voltammetric (CV) responses of nickel, copper, Monel and nickel–copper alloy had been extensively studied and compared in different non-aqueous solvents, such as acetonitrile (AN), propylene carbonate (PC) and sulpholane-containing anhydrous hydrogen fluoride (AHF) medium in the absence and the presence of triethylamine (Et_3N). The quantity of dissolution and surface morphological transformation on the electrodes as a result of anodic polarisation were investigated by means of atomic absorption spectroscopy and scanning electron microscopy (SEM), respectively. The CV study indicates that Ni, Cu and their alloys are highly unstable in AN/AHF medium. Surface morphology of Ni after polarisation in this medium reveals the generation of number of pits, whereas the evolution of small crystallites of CuF_2 is noted on the polarised alloy material, as evidenced by SEM pictures. The dissolution characteristics decrease significantly in PC/AHF medium and become low in sulpholane-containing fluoride medium on the four electrodes. The relative solubility of metal fluoride film in the three solvents increases in the order: sulpholane < PC < AN. The voltammograms suggest that addition of Et_3N (0.5 M) to AN- and PC-containing AHF medium helps both in maintaining uniform dissolution and generating compact fluoride film on the electrode surface. The addition of Et_3N to AHF/sulpholane medium shows only little influence in improving the electrocatalytic oxidation process.

S. Sathyamoorthi · KR. Saravanan · D. Velayutham · V. Suryanarayanan (✉)
CSIR-Central Electrochemical Research Institute, Karaikudi 630006, India
e-mail: vidhyasur@yahoo.co.in; surya@cecri.res.in

Keywords Anodic dissolution · Triethylamine · Passivation · Ni and its alloys · Fluoride film

1 Introduction

Electrochemical perfluorination (ECPF) is one of the frequently used processes for the conversion of organic compounds into their perfluorinated analogues in an industrial scale [1]. This process provides replacement of all hydrogen atoms by fluorine, saturation of double or triple bonds and aromatic systems with fluorine, while functional groups and heteroatoms available in the original molecule are unaffected [2]. The perfluorinated substances produced by ECPF, namely perfluorinated tertiary amines, perfluoroethers, perfluorosulphonic acids and perfluorocarbons, are of prime interest for industry since they are environmentally friendly, non-flammable and fire-safe liquids, applicable as heat carriers, liquid dielectrics, electrolytes and surfactants in wide temperature ranges [3, 4].

On the other hand, ECPF of cycloalkanes and aromatic compounds containing 8–9 or more carbons has not been very successful, as the process often results in the formation of polymeric gums on the electrode surface, thus hindering the use of the continuous electrolysis process [2, 3]. For example, electrolysis of benzotrifluoride could not be performed in the continuous mode due to severe passivation on the anode [5]. An alternative strategy for reducing such electrode fouling is to add suitable additives in the electrolyte which can influence the catalytic activity of electrogenerated NiF_2 film during the course of preparative electrolysis.

Recent literature studies have shown that addition of an alkali metal fluoride such as CsF.2.0HF (50 wt %) in

the electrolyte during the ECPF of $(CH_3)_4NF.4.0HF/Me_3N.3HF$ melt increases the electric conductivity of fluoride film and thereby suppresses the passivation of Ni anode in the voltammetric potential region higher than 3.5 V versus Ag/Ag^+ [6–8]. On the other hand, the addition of a depolariser, namely trialkylamine during the ECPF of octylsulphurylfluoride reveals that the electrolysis can be carried out at sufficiently high-current densities for a longer time and the yield of the final product also increases [9]. In a similar manner, ECPF of toluene and benzotrifluoride occurred in the steady-state mode under the condition of continuous electrolysis with less formation of tarry material in the presence of triallylamine [10]. We also successfully carried out ECPF of aromatic carboxylic acid chlorides containing dimethylsulphide as an additive for preventing anodic fouling [11].

It is important to mention here that the above studies focussed only on the optimisation of preparative electrolysis and product distribution pattern on the ECPF of the fluorinated compounds, and no detailed investigations had been carried out on the characteristic properties of the NiF_2 film generated as a result of electrochemical dissolution of Ni and its alloys, in the presence of tertiary amine within the voltammetric potential region of ECPF reaction (0.0 to 8.0 V vs NHE).

Mechanistic studies [12–14] and [15, 16] reviews have clearly brought out the catalytic roles of electrogenerated NiF_2 and its high-valent fluoride films during the ECPF of organic compounds. Hence, in the present study, the influence of triethylamine (Et_3N) on the electrical conductivity and stability of NiF_2 film was studied by means of cyclic voltammetry in anhydrous hydrogen fluoride (AHF) medium containing the reactants, namely acetonitrile (AN), sulpholane and propylene carbonate (PC). Trifluoroacetonitrile is an important intermediate for the preparation of various biologically active trifluoromethyl derivatives [17–19]. The ECPF of AN [20] and sulpholane [21, 22] on Ni electrode in AHF medium had been well documented in the literature. On the other hand, to our knowledge, no report is available in the literature on the ECPF of PC.

In addition to Ni, two alloy materials, namely Monel (composition of about Ni (66 wt %), Cu (31 wt %)) and Ni–Cu (consisting of about Cu (66 wt %) and Ni (30 wt %)) were taken as the working electrodes in this study. These alloy electrodes are highly corrosion resistant as evidenced by a literature study, where the anodic protection had been provided by evolution of passive NiF_2 film, which is irreducible at potentials less than that of hydrogen evolution [23]. For comparative purpose, Cu had also been used in few studies. Surface morphological characteristics of fluoride films are analysed using scanning electron microscope (SEM) and the amount of metal dissolution by atomic absorption spectroscopic (AAS) technique.

2 Experimental

Preparation of solvents/AHF and solvents/AHF/Et_3N media had been carried out based on our earlier study [24]. The working electrodes were Ni, Cu and their alloys (area was 0.2 cm^{-2}). Compositions of Monel and Ni–Cu alloy were found out from energy dispersive X-ray spectroscopy analysis. The elements found in the Monel and Ni–Cu alloy included: Ni (66.03 wt %) and Cu (31.22 wt %) as well as Ni (30.36 wt %) and Cu (66.45 wt %), respectively, in significant amounts, while Fe, Mn, Co, Al and Si were present only in traces. All the working electrodes except Cu were polished to a mirror finish and washed repeatedly with triple-distilled water followed by trichloroethylene before use. Since an insoluble film is formed during each potential cycle, these electrodes had to be repeatedly cleaned and polished after each cyclic voltammetric (CV) experiment in order to get reproducible results.

The choice of reference electrode posed some problems. The palladium (Pd/H_2) electrode showed instability, especially in fluoride medium in which Pd dissolution was noticed. Hence, a Pt wire was used as a quasi-reference electrode. In our previous studies involving anodic polarisation on Ni, Ag and Cu in AHF medium, Pt had been used as the quasi reference and no appreciable potential drift was observed [24–27]. The measurements suggested that the Pt quasi reference potential in fluoride medium was always close to the Pd/H_2 reference electrode within the limit of ± 20 to ± 30 mV. However, as a precautionary measure, the reference potential was checked from time to time externally against a saturated calomel electrode. A Pt foil as counter electrode in a polypropylene undivided cell was used throughout the study. AN (high-performance liquid chromatography grade), PC [analytical reagent (AR) grade], sulpholane (AR grade) and triple-distilled water were used as solvents.

Voltammetric measurements were carried out using an Autolab PGSTAT302N system under computer control. SEM was performed with JEOL, model 30CF instrument. The amount of Ni^{2+} and Cu^{2+} species dissolved in the electrolyte was estimated using AAS (GBC 906 AA, and Australia). For the AAS analysis, the working electrodes were anodically polarised in solvents/AHF and solvents/AHF/Et_3N media at a slow sweep rate of 40 mV s^{-1} within the corresponding potential limit (five cycles). After polarisation, 0.25 ml of the electrolyte was pipetted out and made up to 10 ml using triple-distilled water, and this diluted portion was subjected for AAS analysis. All the experiments were carried out at 303 ± 1 K.

3 Results and discussion

3.1 CV studies in solvents containing 3.0 M AHF

Typical multisweep CVs of Ni, Monel and Ni–Cu alloy electrodes in AN-containing 3.0 M AHF recorded within a potential limit of −0.8 to 8.0 V, versus Pt at a constant sweep rate of 40 mV s^{-1} are shown in Fig. 1a–c, respectively. Different voltammetric parameters such as anodic peak potential (E_{pa}) and initiation potential (E_i) at which the current rises after dissolution, and anodic charge densities namely Q_a and Q_{a1} are indicated in Table 1. As Cu shows very severe dissolution in this medium, no reproducible voltammograms had been recorded. On Ni electrode, the current–potential curve shows a linear increase initially, followed by a sharp peak at a peak potential of 4.65 V, and then falls suddenly. With increase in potential beyond 4.65 V, a second dissolution process starts, where the current increases like a ramp up to 7.0 V and then decreases drastically to the initial current value. In the reverse scan, no cathodic reduction peak is noted. In all subsequent sweeps, the dissolution current is totally absent indicating the passivation of the electrode surface.

The irreversible process is associated with dissolution of Ni to Ni^{2+}, followed by the precipitation of Ni^{2+} to NiF_2-resistive film. The dissolution curves obtained in the present case are essentially corresponding to the dissolution–precipitation model of resistive film formation, which is more commonly known as Muller's passivation model. The voltammetric characteristics corresponding to this model had already been derived and experimentally verified in the earlier literatures [28]. The model as well as the CV method corresponding to such a dissolution–precipitation process had also been discussed [29].

The linear current–potential curve region in the voltammetric curves corresponds to the resistivity to charge transfer. The resistivity is due to pore-resistance of Muller's passivation model, in the potential region before peak potential, and after the peak potential region, this resistivity has been offered by NiF_2 film formed on the electrode surface. The NiF_2 film formed during the first anodic sweep is fairly stable and is even highly insoluble in AN. As a result of this, the dissolution charge and the peak current are completely absent in subsequent sweeps. The appearance of a second voltammetric process beyond 4.65 V may be due to the non-uniform dissolution process taking place on the pits of the metal surface generated as a result of severe dissolution in the AN/AHF medium (the dissolution charge density is 7077.5 mC cm^{-2}, Table 1).

Monel (Fig. 1b) and Ni–Cu alloy (Fig. 1c) electrodes retain both the passivity and irreversibility, a similar behaviour exhibited by Ni, to a greater extent. Monel gets oxidised comparatively at lesser positive potential than Ni; however, a very high potential is needed for the

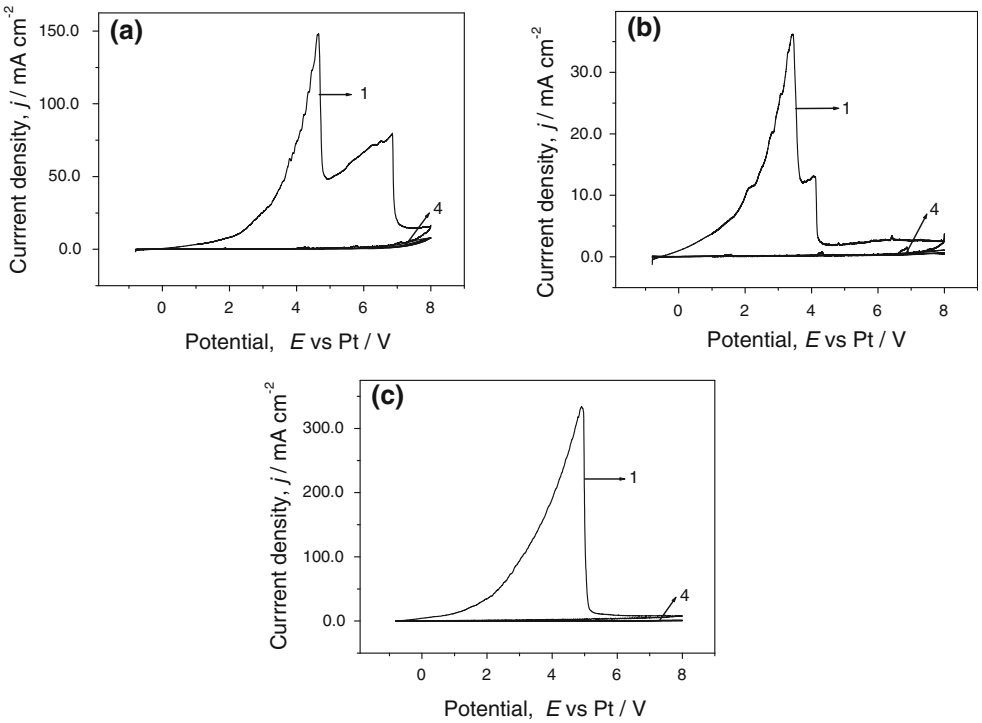

Fig. 1 Multisweep cyclic voltammograms of: **a** Ni, **b** Monel and **c** Ni–Cu alloy in AN-containing 3.0 M AHF at a sweep rate of 40 mV s^{-1}. Number of cycles = 4

Table 1 Voltammetric characteristics of Ni, Cu and their alloys in different solvents containing AHF (3.0 M) at a sweep rate of 40 mV s^{-1}

Solvent/ AHF	Electrode	E_{pa} (V)	E_i (V)	Q_a (mC cm^{-2})	Q_{a1} (mC cm^{-2})
AN	Ni	4.65	–	7077.5	–
	Monel	3.45	–	1121.1	–
	Ni–Cu alloy	4.91	–	12340.0	–
PC	Ni	2.58	3.64	526.0	816.5
	Monel	2.47	4.03	408.8	218.9
	Ni–Cu alloy	2.12	4.10	253.5	110.3
	Cu	2.77	–	542.0	–
Sulpholane	Ni	−0.14	2.52	2.6	377.3
	Monel	0.30	4.03	12.4	100.4
	Ni–Cu alloy	0.28	–	14.0	–
	Cu	1.17	–	79.6	–

electrooxidation of Ni–Cu alloy. This can also be reflected in the high Q_a value obtained for Ni–Cu alloy when compared to Ni and Monel electrodes (Table 1). This shows that significant amount of Cu content may lead to a high-dissolution process at an elevated potential. It is important to mention here that the contribution by the second dissolution process is found to be very low on Monel electrode and is even completely absent in Ni–Cu alloy which is associated with the partial contribution of uniform dissolution of Cu over the surface of Ni. Once again, there is no dissolution current in the subsequent sweeps within the potential limit of 8.0 V, and for the three electrodes, E_i value is almost zero in this medium.

Similar types of voltammograms had been obtained for these four electrodes in PC-containing 3.0 M AHF. Multisweep CVs recorded for Ni, Monel, Ni–Cu alloy and Cu in PC/AHF at a sweep rate of 40 mV s^{-1} are shown in Fig. 2a–d, respectively. The two electrochemical processes, namely the NiF_2 film formation and the Ni(II) oxidation/fluorination evolution regions, are close to each other. The anodic oxidation of Ni and its alloys takes place at lesser positive potential than that of AN/AHF medium, and the Q_a value also decreases substantially (Table 1). However, the second dissolution pattern, noted in the case of AN/AHF, is completely absent in this medium. Once again, in the reverse scan, no cathodic reduction peak is noted. The E_i value is at 3.64 V for Ni and is approximately 4.0 V for its alloys. However, in all subsequent sweeps, complete passivation follows up to 4.0 V, and beyond this a steep rise of current plateau is noticed (Fig. 2a–c), where Ni shows higher charge density (Q_{a1}) than the other electrodes for this process (Table 1). In the case of Cu electrode, anodic oxidation takes place slightly at higher potential than the other electrodes and dissolution current still persists in the subsequent sweeps (Fig. 2d). This leads to a fact that the resultant CuF_2 film is highly soluble in this solvent-supporting electrolyte system, leading to the fresh dissolution of Cu with successive polarisations.

Voltammograms obtained for these four electrodes were found to be totally different when polarised in sulpholane-containing 3.0 M AHF solution under identical experimental conditions. The two electrochemical processes, mentioned in the above discussion, are well separated. The dissolution process takes place at a negative potential of −0.14 V and the dissolution charge density also becomes low (Fig. 3a; Table 1). Surprisingly, the E_i value starts itself earlier (2.52 V, Table 1) in the first and subsequent sweeps. The fluoride film formation occurs at more positive potentials for Monel and Ni–Cu alloy electrodes than that of the Ni (Fig. 3b, c). However, E_i value is found to increase beyond 4.0 V for Monel and is totally absent for Ni–Cu alloy. The electrode passivity has been still maintained in these three electrodes with successive scans and no cathodic current is noticed in the reverse scan. The anodic oxidation for Cu starts at higher positive potential than that of the other three electrodes with very high dissolution charge density (Table 1; Fig. 3d).

It is understandable that among the three solvents and four electrodes investigated so far, the catalytic fluorine evolution current rises sharply in PC- and sulpholane-containing AHF media on the anodic polarisation of Ni and its alloys. In PC/AHF medium, even the charge density obtained for the fluoride film formation is found to be low. Overall, it is important to note that among the different solvents containing AHF, the anodic dissolution charge density of the electrodes increases in the order: sulpholane < PC < AN. The highest charge density noted in AN/AHF medium originates not only through electrochemical pathway, but also by chemical route leading to the formation of blue coloured $Ni(CH_3CN)_2F_2$ complex along with NiF_2 film, as evidenced by a previous report [30]. On the other hand, no such chemical dissolution takes place during the anodic polarisation of Ni in sulpholane/AHF medium, as this solvent forms a thin uniform composite layer on the nickel fluoride surface and this film prevents further dissolution of nickel [26]. Further investigations on the anodic polarisation of the above electrode materials, in the AHF medium without solvents, will throw some light on the mechanistic pathways, which will be our future study on this topic. Since Cu shows severe anodic dissolution in AN/AHF medium and complete passivation is not observed during the subsequent voltammetric sweeps recorded in PC and sulpholane media, further voltammetric studies are carried out only on Ni and its alloys.

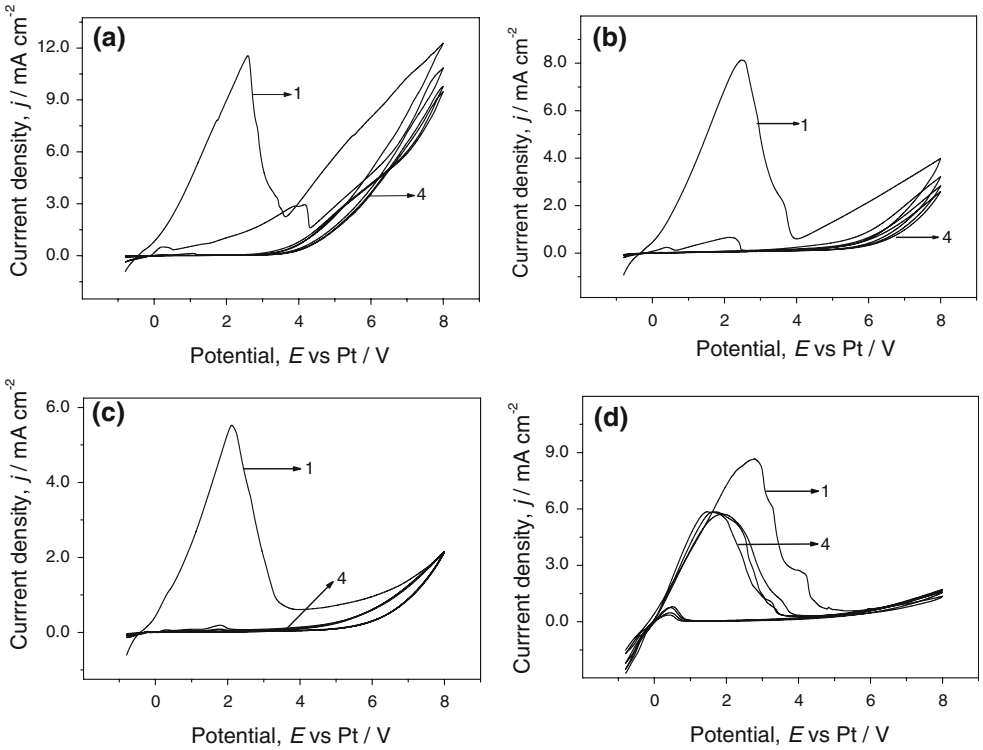

Fig. 2 Multisweep cyclic voltammograms of: **a** Ni, **b** Monel, **c** Ni–Cu alloy and **d** Cu in PC-containing 3.0 M AHF at a sweep rate of 40 mV s^{-1}. Number of cycles = 4

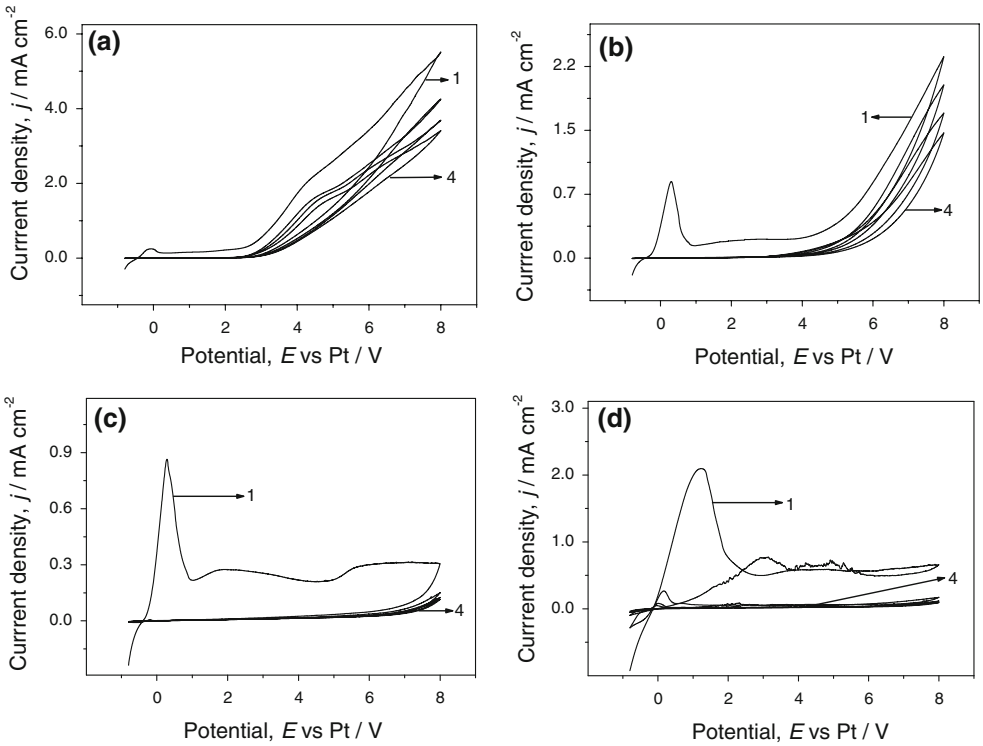

Fig. 3 Multisweep cyclic voltammograms of: **a** Ni, **b** Monel, **c** Ni–Cu alloy and **d** Cu in sulpholane-containing 3.0 M AHF at a sweep rate of 40 mV s^{-1}. Number of cycles = 4

3.2 CV studies on the effect of addition of Et_3N (0.5 and 1.0 M) to solvents containing 3.0 M AHF

The voltammograms changed drastically during the addition of Et_3N to AN/AHF solvent medium. Typical multisweep CVs of Ni in AN-containing 3.0 M AHF and Et_3N (0.5 M) at a sweep rate of 40 mV s^{-1} are shown in Fig. 4a. A small anodic peak is observed at −0.48 V with a charge density of 13.1 mC cm^{-2}, which is associated with NiF_2 film formation [24]. This is followed by a steadily increasing current beyond 1.85 V. The peak potential for this peak, however, is not distinct and the calculated charge density for this process is very high (4,102 mC cm^{-2}) (Fig. 4a). In the subsequent sweeps, complete passivation exists up to 6.0 V and beyond this, the gas evolution current rises sharply. The voltammetric patterns obtained for the Monel and Ni–Cu alloy under these conditions were almost similar. For example, one sharp oxidation peak is found out approximately at −0.14 V for Monel electrode and beyond this, the current does not rise sharply (Fig. 4b). The anodic dissolution charge for this peak increases drastically with increase of Cu content (from 145 to 1,420 mC cm^{-2}) indicating the enhanced solubility of both NiF_2 and CuF_2 in AN/AHF-containing Et_3N (Table 2).

On further addition of Et_3N (1.0 M), significant changes in the voltammetric pattern were noted for these three electrodes. For example, on Ni, the peak potential for the fluoride film occurs at a high positive potential of 1.88 V and the dissolution charge density further decreases (Fig. 4c; Table 3). The second anodic process, associated with the electrooxidation of Ni(II) component to Ni(III) or Ni(IV) species, is initiated beyond 4.0 V for all the three electrodes. It is important to mention here that the dissolution charge density for the fluoride film formation on Monel and Ni–Cu alloy decreases drastically with the addition of Et_3N. The formation of CuF_2 film along with NiF_2 layer prevents the electrooxidation of Ni(II) to a higher oxidation state and as a result of this, the anodic charge density for the these electrochemical processes (Q_{a1}) also decreases with the increase in Cu content. With subsequent sweeps, passivation of electrode surface still exists and the fluorine evolution current could be clearly observed beyond 4.0 V on all the three electrodes. On further addition of Et_3N, no considerable changes in the CVs of three electrodes are noted.

The voltammograms of Ni and Monel recorded in PC-containing Et_3N (0.5 M) exhibit an anodic peak at potentials of 0.12 and 0.30 V, respectively, corresponding to their metal fluoride film formation (Fig. 5a, b). The dissolution charge density for the above process is lesser than those obtained in the absence of Et_3N. The second anodic process proceeds with high charge density for Ni, moderate for Monel electrode and very low on Ni–Cu alloy (Table 2). With more addition of Et_3N (1.0 M), the charge density corresponding to the fluoride film formation decreases significantly on Ni (Fig. 5c), Monel and Ni–Cu

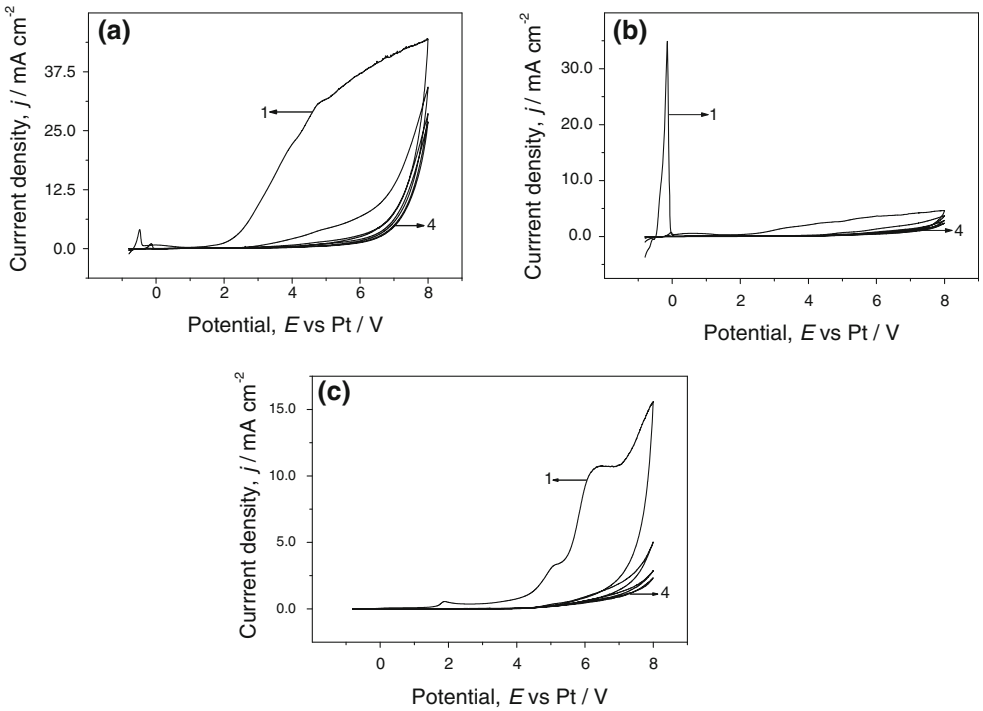

Fig. 4 Multisweep cyclic voltammograms of: **a** Ni and **b** Monel in AN-containing 3.0 M AHF/0.5 M Et_3N and **c** Ni in AN-containing 3.0 M AHF/1.0 M Et_3N at a sweep rate of 40 mV s^{-1}. Number of cycles = 4

alloy electrodes. The initiation potential for the second electrochemical process increases with an increment of more than 1.0 V. The charge density for the fluoride film formation increases with the increase of Cu content and with subsequent addition of Et_3N (Table 3).

It is interesting to note that during the first anodic process,, the region of the fluoride film formation is not clearly seen in the multisweep voltammograms of Ni and Monel obtained in presence of Et_3N (0.5 M) containing sulpholane/AHF medium (Fig. 6a, b). Charge density value for the second anodic process increases slightly with the addition of Et_3N, however, the E_i remains the same (Table 2). Once again, the Q_{a1} value for the second electrochemical process decreases with the increase of Cu content. With further addition (1.0 M), the current plateau shifts towards the positive value on all the electrodes (Fig. 6c) and there is not much change in the voltammetric pattern.

Table 2 Voltammetric characteristics of Ni and its alloys in different solvents containing AHF (3.0 M) in the presence of Et_3N (0.5 M) at a sweep rate of 40 mV s^{-1}

Solvent/ AHF/Et_3N	Electrode	E_{pa} (V)	E_i (V)	Q_a (mC cm^{-2})	Q_{a1} (mC cm^{-2})
AN	Ni	−0.48	1.85	13.1	4102.5
	Monel	−0.14	2.37	145.1	403.0
	Ni–Cu alloy	−0.18	–	1419.8	–
PC	Ni	0.12	2.34	25.1	3097.5
	Monel	0.30	3.13	41.5	316.8
	Ni–Cu alloy	0.29	–	84.2	–
Sulpholane	Ni	–	2.78	–	584.8
	Monel	0.19	4.50	1.8	117.6
	Ni–Cu alloy	0.01	4.66	2.6	67.7

Table 3 Voltammetric characteristics of Ni and its alloys in different solvents containing AHF (3.0 M) in presence of Et_3N (1.0 M) at a sweep rate of 40 mV s^{-1}

Solvent/ AHF/Et_3N	Electrode	E_{pa} (V)	E_i (V)	Q_a (mC cm^{-2})	Q_{a1} (mC cm^{-2})
AN	Ni	1.88	4.13	8.0	439.5
	Monel	1.90	4.03	15.0	231.1
	Ni–Cu alloy	1.98	4.07	20.0	151.3
PC	Ni	−0.19	3.54	1.6	1891.5
	Monel	−0.14	4.67	2.6	238.8
	Ni–Cu alloy	0.13	5.28	7.0	121.6
Sulpholane	Ni	2.12	3.27	0.8	326.5
	Monel	2.25	4.60	1.3	123.5
	Ni–Cu alloy	2.28	4.91	1.8	62.1

The controlled dissolution of Ni and its alloys in the AN- and PC-containing AHF media in the presence of Et_3N may be explained as follows.

For effective anodic dissolution of Ni, both acidity and high fluoride ion concentration are essential. Acidity is required for chemically converting the nickel hydroxyl or oxide layer into electrochemically active nickel oxy fluoride or fluoride layer.

In solvents containing AHF medium, this chemical initiation is possible to some extent by the self-dissociation of HF

$$2HF \rightarrow H^+ + HF_2{}^-. \quad (1)$$

Et_3N addition in a small ratio, for example, leads to further dissociation of HF leading to enhanced fluoride ion concentration [31]

$$Et_3N + 2HF \rightarrow Et_3NH^+ + HF_2{}^-. \quad (2)$$

On the other hand, the above reaction decreases the effective H^+ ion concentration which slows down the formation of electrochemical active nickel oxyfluoride (Eq 2), leading to a decrease in the dissolution of metals. Further addition of Et_3N completely suppresses the formation H^+ ion concentration and totally controls the metal dissolution process. Furthermore, this phenomenon is responsible for the shift of the potential of the first anodic processes to more positive value. As the dissolution charge densities noted for Ni and its alloys are already very low in AHF/sulpholane when compared to the same in AN/AHF and PC/AHF media (Table 1), the enhanced fluoride ion concentration shows little influence on their further dissolution.

3.3 Surface characterisation by SEM

Microscopic images of Ni at two different magnifications, (a) and (b), Monel (c), and Ni–Cu alloy (d) at one magnification obtained after potentiostatic polarisation at 7.0 V for 5 min in AN-containing AHF medium, are shown in Fig. 7. Appearance of large pits at very low magnification (Fig. 7a) and ring-like patterns at slightly high magnification (Fig. 7b) ensure the severe Ni dissolution/NiF_2 passivation behaviour, confirming the earlier results [24]. On Monel electrode (with 31.22 % of Cu), the pitting pattern completely disappears and the evolution of small crystallites of CuF_2 is noted on the scratched line as a result of the Cu dissolution and CuF_2 precipitation along with NiF_2 crystallites (Fig. 7c). Further increase of Cu (66.45 % of Cu in Ni–Cu alloy) leads to an increase in the number of CuF_2 crystallites (Fig. 7d). As mentioned earlier, the SEM

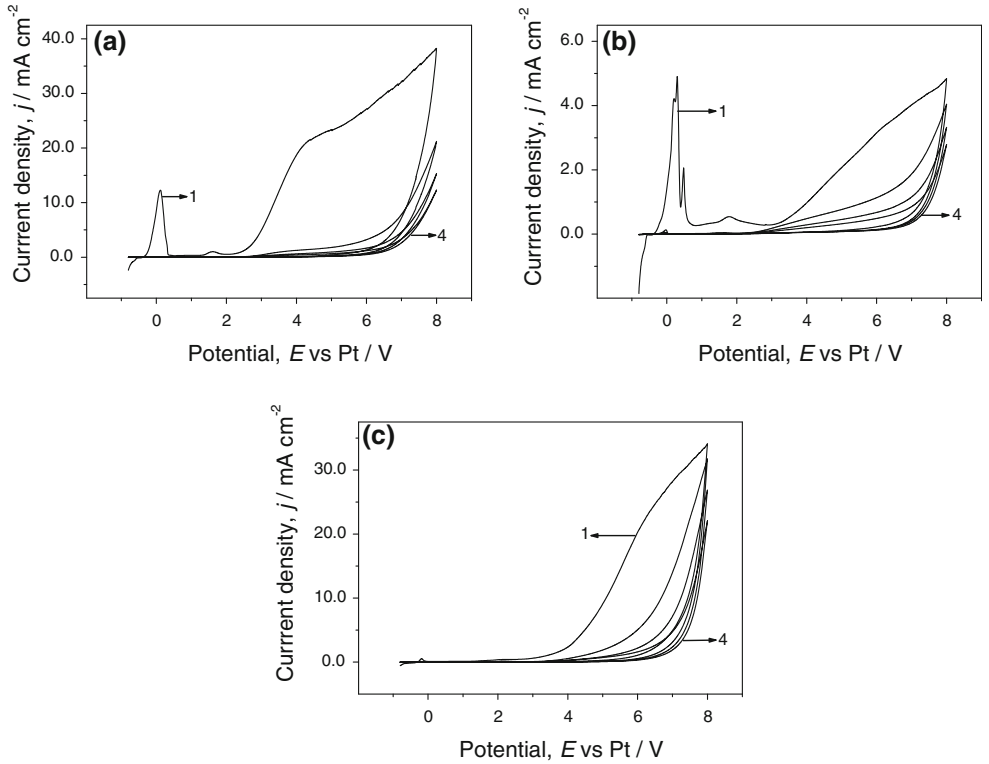

Fig. 5 Multisweep cyclic voltammograms of: **a** Ni and **b** Monel in PC-containing 3.0 M AHF/0.5 M Et_3N and **c** Ni in PC-containing 3.0 M AHF/1.0 M Et_3N at a sweep rate of 40 mV s^{-1}. Number of cycles = 4

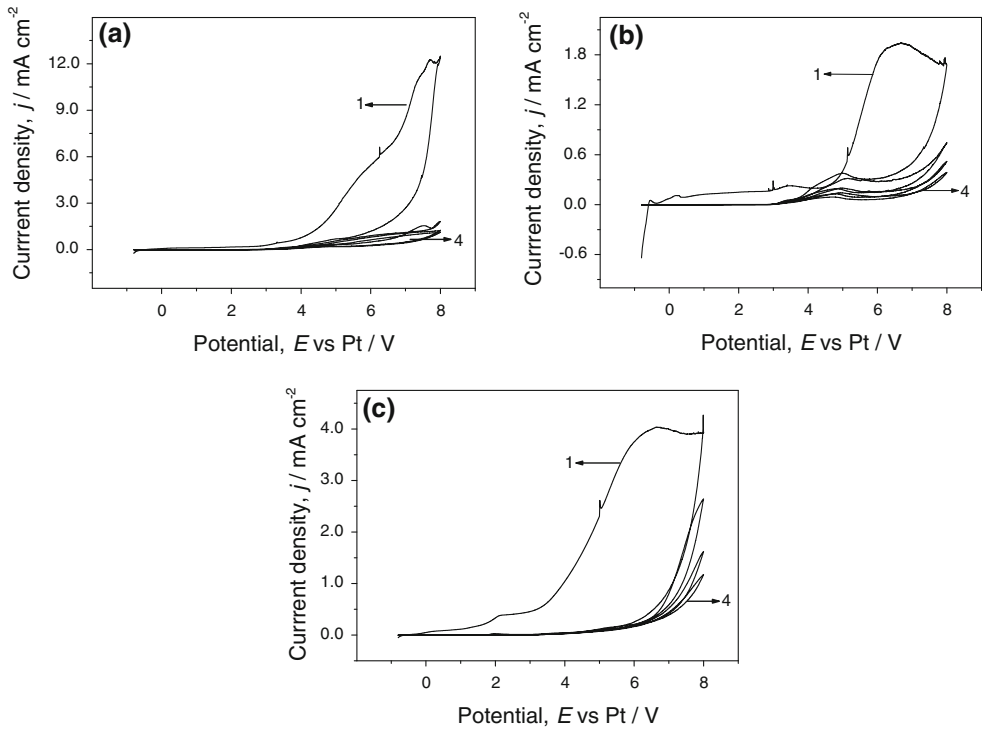

Fig. 6 Multisweep cyclic voltammograms of: **a** Ni and **b** Monel in sulpholane-containing 3.0 M AHF/0.5 M Et_3N and **c** Ni in sulpholane-containing 3.0 M AHF/1.0 M Et_3N at a sweep rate of 40 mV s^{-1}. Number of cycles = 4

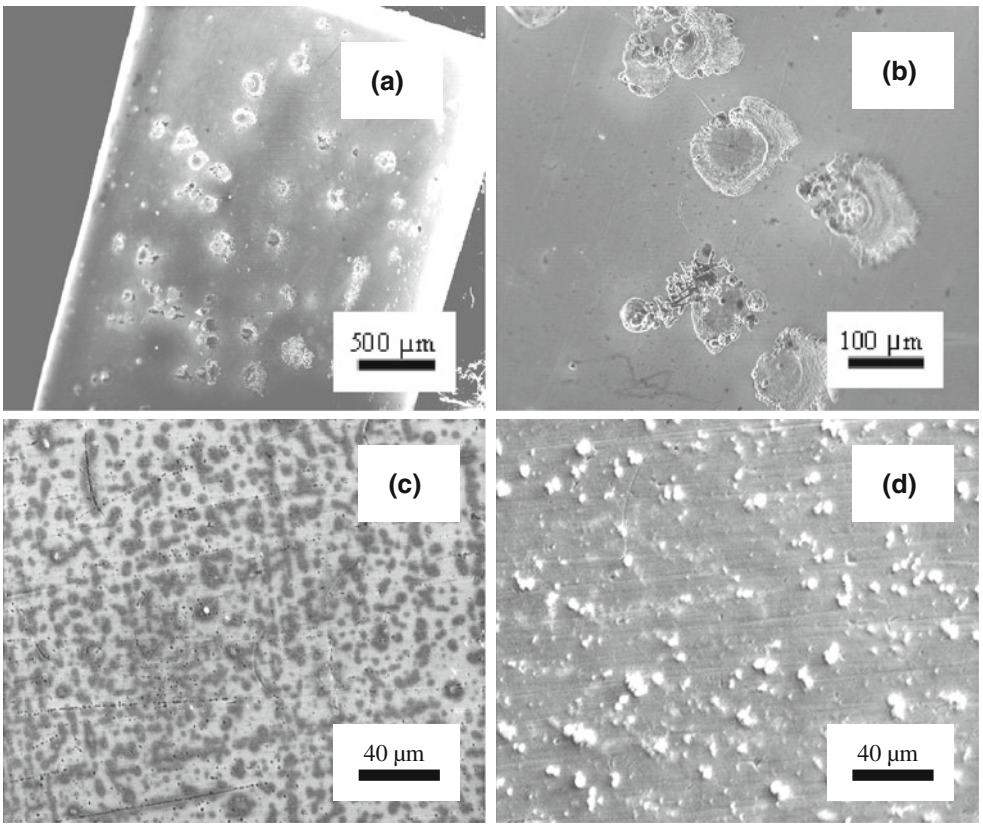

Fig. 7 SEM images of: **a** and **b** Ni, **c** Monel and **d** Ni–Cu alloy obtained after anodic polarisation for 5 min at 7.0 V in AN-containing 3.0 M AHF. Magnification: **a** ×39, **b** ×200, **c** and **d** ×500

pictures of Cu electrode, obtained after the polarisation in AN-containing fluoride medium, are found to be featureless as the electrode undergoes severe dissolution. Furthermore, the morphology of electrodes polarised in PC/AHF medium are similar with that of AN/AHF medium. Hence, the corresponding morphological pictures are not shown here.

All the four electrodes exhibit remarkable stability during the anodic polarisation in sulpholane-containing AHF medium. Typical SEM pictures of the four polarised electrodes obtained in sulpholane medium are presented in Fig. 8. Under the identical polarisation conditions, Ni exhibits uniform dissolution and compact NiF_2 film formation without any pit on the electrode surface (Fig. 8a). Formation of CuF_2 bulk phase over NiF_2 layer is visible (Fig. 8b). Further increase of Cu content leads to the formation of few CuF_2 crystallites along with more number of pits (Fig. 8c). A large number of CuF_2 crystallite as clusters are discovered on the Cu surface (Fig. 8d).

Microscopic pictures of Ni electrode obtained after the anodic polarisation in Et_3N (0.5 M) containing AN/AHF medium lead to the evolution of uniform dissolution of Ni surface followed by the formation compact NiF_2 film (Fig. 9a). A few pits are, however, seen in the background (Fig. 9a). With more amount of the Et_3N (1.0 M), pit formation is not predominant and appearance of more NiF_2 salts as clusters one-over-the-other are noted (Fig. 9b). The anodic polarisation of Monel and Ni–Cu alloy under this same condition leads to the evolution of different structural morphology. Monel shows formation of tiny crystals of CuF_2 over compact NiF_2 film (Fig. 9c) and Ni–Cu alloy reveals uniform dissolution with occasional pits (Fig. 9d). The structural pattern of the electrodes polarised in Et_3N/PC/AHF medium are almost similar with that of Et_3N/AN/AHF medium and there are no specific changes in morphological characteristics of the electrodes obtained after the addition of amine in sulpholane/AHF medium.

3.4 Metal dissolution by AAS studies

The AAS analysis also provides some interesting insights on the relationship between dissolution charge density and quantity of metal dissolved in the electrolyte. Furthermore, this analysis also helps to understand the influence of the addition of Et_3N on dissolution of metals. Based on the CV and SEM analyses, AAS analysis was carried out only on

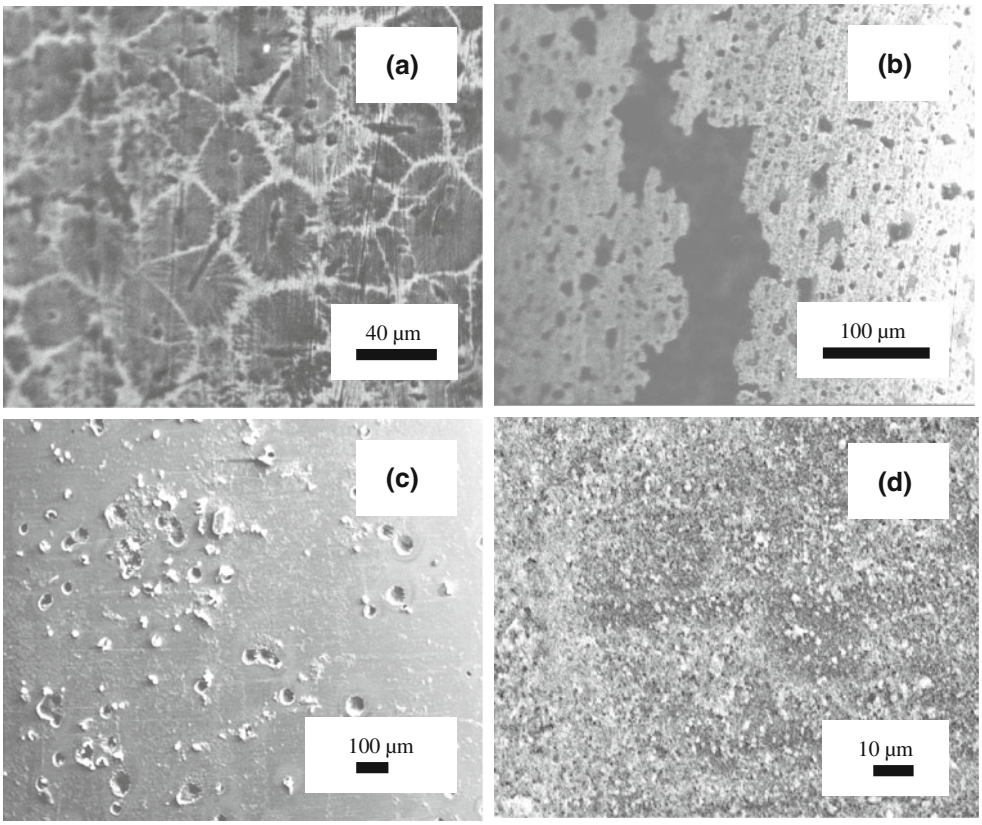

Fig. 8 SEM images of: **a** Ni, **b** Monel, **c** Ni–Cu alloy and **d** Cu obtained after anodic polarisation for 5 min at 7.0 V in sulpholane-containing 3.0 M AHF. Magnification: **a** ×500, **b** and **c** ×100 and **d** ×1000

Ni and Monel electrodes in AN/AHF medium with and without Et_3N, as well as in fluoride ion-containing PC and sulpholane media. The AAS analysis of AN/AHF medium obtained after the anodic polarisation of Ni shows the highest amount of Ni and this is associated with its severe dissolution as reflected from their high Q_a value (Table 4). However, the amount of Ni present in the same solution is found to be very low when the electrode is Monel. By adding Et_3N (0.5 M) to this medium, the quantity of dissolved Ni decreases drastically. This confirms that the presence of Et_3N is necessary in controlling the exhaustive dissolution of Ni and Monel in AN/AHF medium. The next addition still lowers the amount of Ni and Cu in the electrolyte (Table 4). On the other hand, the quantity of Ni is found to be very low in sulpholane/AHF medium containing polarised Ni and Monel (Table 4). This shows that in this medium, the addition of Et_3N is unnecessary.

The earlier literature works carried out on the anodic polarisation of Ni electrode in the fluoride melt, clearly showed that the electrochemical fluorination reaction took place in between 4.0 and 8.0 V versus Ag/Ag^+, which was associated with two anodic processes namely electrocatalytic oxidation of Ni(II) fluoride to Ni(III) or Ni(IV) and fluorine evolution reaction, respectively [6–8]. Furthermore, the above voltammetric analysis revealed that the potential region of NiF_2 film formation and the above plateau current are well separated by a value of 4.0 V versus Ag/Ag^+. Based on these results, it is concluded that in the present study, the sulpholane/AHF medium in the absence of Et_3N, exhibits good electrocatalytic behaviour on both Ni and Monel electrodes with considerable anodic charge in both regions of fluoride film formation and Ni(II) oxidation.

On the other hand, as revealed by CV and SEM investigations, the stability of the four electrodes in AN- and PC-containing AHF medium is found to be very low, and the addition of 0.5 M of Et_3N to these solvent systems could somehow control the exhaustive dissolution of metals. It is understandable that the additive helps to generate compact metal fluoride film on the electrode surface and improves the separation of the potential regions between fluoride film formation region and oxidation of Ni(II) species. It also helps to improve the catalytic current quantitatively beyond 4.0 V in these two solvent systems.

Further works are in progress in carrying out the preparative electrolysis of AN-, PC- and sulpholane-containing AHF medium in the presence and the absence of Et_3N on Ni and Monel electrodes, and the products will be characterised. Moreover, in-depth surface characterisation of Ni and its alloys after electrolysis must be necessary in

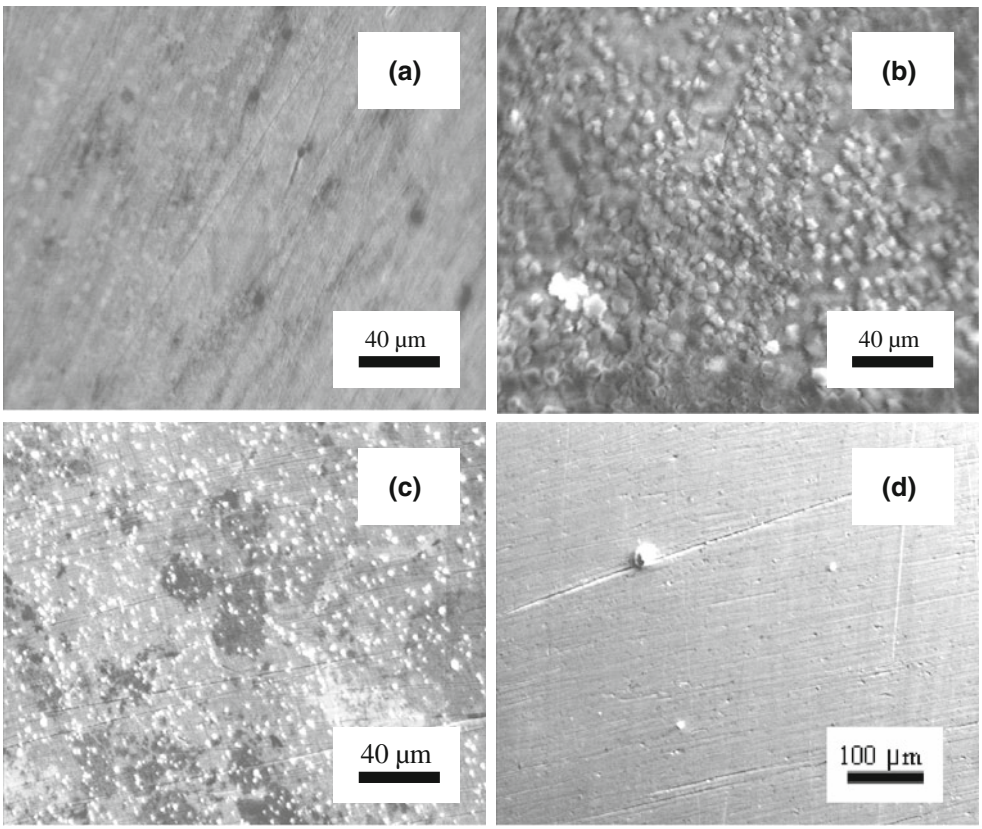

Fig. 9 SEM images of: **a** and **b** Ni, **c** Monel and **d** Ni–Cu alloy obtained after anodic polarisation for 5 min at 7.0 V in AN/3.0 M AHF-containing: **a** 0.5 M and **b–d** 1.0 M Et_3N. Magnification: **a** and **b** ×1000, **b** ×500 and **d** ×200

Table 4 AAS data for dissolved metal species obtained after the anodic polarisation of Ni and Monel in solvents containing AHF (3.0 M) in the absence and the presence of Et_3N

Solvent/AHF	Electrode	Ni (μM)	Cu (μM)
AN	Nickel	26.85	Nil
	Monel	3.86	0.55
Et_3N[a]/AN	Nickel	1.62	Nil
	Monel	0.72	0.10
Et_3N[b]/AN	Nickel	0.01	Nil
	Monel	0.03	Not detectable
Sulpholane	Nickel	1.87	Nil
	Monel	0.18	0.08

[a] Concentration of Et_3N is 0.5 M

[b] Concentration of Et_3N is 1.0 M

order to find out the stability of the fluoride films formed on the electrodes.

4 Conclusions

The present study indicates clearly the role of solvents and the acid–base relationship of the electrolyte (HF–amine ratio) on the anodic dissolution of Ni, Cu and their alloys. In AN/AHF medium, Ni and Ni–Cu alloy show exhaustive dissolution/passivation behaviour in the voltammetric potential region of 8.0 V versus Pt. The film dissolution on Ni occurs through pits, generated in the active/passive region and on its alloys with the evolution of both NiF_2/CuF_2 crystallites as noted from the SEM pictures. The dissolution characteristics decrease significantly in PC/AHF and become low in sulpholane-containing fluoride medium on the four electrodes. In the three solvents, the solubility of the fluoride film of Ni and Cu increases with the increase of Cu content. An addition of 0.5 M of Et_3N to AN- and PC-containing fluoride media enhances the fluoride ion concentration. As a result of this, the exhaustive dissolution of the electrode material decreases, as confirmed from SEM studies and AAS analysis. Further addition lowers the charge density not only on the oxidative dissolution of Ni, but also the electrocatalytic oxidation of Ni(II) to Ni high valent species. The presence of Et_3N in sulpholane/AHF medium shows only little influence in improving the film growth and the electrooxidation process.

Acknowledgments The authors thank Director, CSIR-CECRI, Karaikudi for his keen encouragement in publishing this work. Financial support from DRDO, New Delhi is greatly acknowledged. Thanks are due to Dr. R.P. Singh and Dr. Raju Brahma, CFEES, DRDO, New Delhi for their fruitful discussions.

References

1. Alsmeyer YW, Childs WV, Flynn RM, Moore GGI, Smeltzer JC (1994) In: Banks RE, Smart BE, Tatlow JC (eds) Organic fluorine chemistry: principles and commercial applications. Plenum, New York
2. Childs WV, Christensen L, Klink FW, Koplin CF (1991) In: Lund H, Baizer MM (eds) Organic electrochemistry, 3rd edn. Marcel Dekker, New York
3. Chambers RD (2004) Fluorine in organic chemistry. Blackwell, Oxford
4. Jayaraman K, Noel M (2001) Bull Electrochem 17:227–238
5. Yonekura M, Nagase S, Baba H (1976) Bull Chem Soc Jpn 49:1113–1116
6. Shodai Y, Inaba M, Momota K, Kimura T, Tasaka A (2004) Electrochim Acta 49:2131–2137
7. Tasaka A, Yachi T, Makino T, Hamano K, Kimura T, Momota K (1999) J Fluor Chem 97:253–261
8. Tasaka A, Nakanishi K, Masuda N, Nakai T, Ikeda K, Momota K, Saito M, Inaba M (2011) Electrochim Acta 56:4335–4343
9. Matalin VA, Kaurova GI, Moldavskiy DD, Barabanov VG, Blinova OV (2003) Fluor Notes 6:31–35
10. Matalin VA, Kaurova GI, Berenblit VV, Gribel VI (2007) Russ J Appl Chem 80:2090–2092
11. Ilayaraja N, Velayutham D, Noel M (2009) J Fluor Chem 130:656–661
12. Dimitrov A, Rudiger S, Seppelt K, Peplinski T (1994) J Fluor Chem 69:15–19
13. Rudiger S, Dimitrov A, Hottman K (1996) J Fluor Chem 76: 155–160
14. Sartori P, Ignat'ev N, Datsenko S (1995) J Fluor Chem 75: 157–161
15. Sartori P, Ignat'ev N (1998) J Fluor Chem 87:157–162
16. Drakesmith FG (1997) Electro fluorination of organic compounds. Springer, Berlin
17. Sing YL, Lee LF (1985) J Org Chem 50:4642–4646
18. Lee LF, Stikes GL, Sing YL, Miller ML, Dolson MG, Normansell JE, Auinbauh SM (1991) Pestic Sci 31:555–568
19. Parker MH (2004) Synth Commun 34:903–907
20. Haruta M, Watanabe N (1976) J Fluor Chem 7:159–177
21. Rozhkov IN, Bukhtiarov AV, Knunyants L (1969) Izv Akad Nauuk SSSR Ser Chem 4:945–947
22. Bulan A, Herzig J (2004) US Patent: US 6752917
23. Qian SY, Dumont H, Conway BE (1997) J Appl Electrochem 27:1245–1253
24. Noel M, Suryanarayanan V, Krishnamoorthy S (1995) J Fluor Chem 74:241–246
25. Noel M, Suriyanarayanan N, Suryanarayanan V (2001) J Solid State Electrochem 5:419–430
26. Suriyanarayanan N, Noel M (2008) J Solid State Electrochem 12:1453–1460
27. Sathyamoorthi S, Velayutham D, Suryanarayanan V, Noel M (2011) Electrochim Acta 56:7012–7021
28. Calandra AJ, DeTacconi NR, Perevio R, Arvia AJ (1974) Electrochim Acta 19:901–905
29. Noel M, Vasu KI (1990) Cyclic voltammetry and the frontiers of electrochemistry. Oxford-IBH, New Delhi
30. Clifford AF, Sargent J (1957) J Am Chem Soc 79:4041–4045
31. Isogai T, Nakai T, Inoue H, Nakanishi K, Kohara S, Saito M, Inaba M, Tasaka A (2011) J Phys Chem B 115:9593–9603